Semiannual Technical Report

Low Temperature Deposition and Characterization of N- and P-Type Silicon Carbide Thin Films and Associated Ohmic and Schottky Contacts

Supported under Grant #N00014-92-J-1500
Office of the Chief of Naval Research
Report for the period 1/1/95–6/30/95

R. F. Davis and R. J. Nemanich*
O. Aboelfotoh, J. P. Barnak*, M. C. Benjamin*, S. Kern,
S. W. King and L. M. Porter
Materials Science and Engineering Department
*Department of Physics
North Carolina State University
Raleigh, NC 27695

June, 1995

REPORT DOCUMENTATION PAGE

Form Approved
OMB No. 0704-0188

1. AGENCY USE ONLY *(Leave blank)*	2. REPORT DATE	3. REPORT TYPE AND DATES COVERED
	June, 1995	Semiannual Technical 1/1/95-6/30/95

4. TITLE AND SUBTITLE

Low Temperature Deposition and Characterization of N- and P-Type Silicon Carbide Thin Films and Associated Ohmic and Schottky Contacts

5. FUNDING NUMBERS

sic0002---02
1261
N00179
N66005
4B855

6. AUTHOR(S)

Robert F. Davis and Robert J. Nemanich

7. PERFORMING ORGANIZATION NAME(S) AND ADDRESS(ES)

North Carolina State University
Hillsborough Street
Raleigh, NC 27695

8. PERFORMING ORGANIZATION REPORT NUMBER

N00014-92-J-1500

9. SPONSORING/MONITORING AGENCY NAMES(S) AND ADDRESS(ES)

Sponsoring: ONR, Code 1261, 800 N. Quincy, Arlington, VA 22217-5660
Monitoring: Administrative Contracting Officer, ONR Regional Office Atlanta
101 Marietta Tower, Suite 2805
101 Marietta Street
Atlanta, GA 30332-0490

10. SPONSORING/MONITORING AGENCY REPORT NUMBER

11. SUPPLEMENTARY NOTES

12a. DISTRIBUTION/AVAILABILITY STATEMENT

Approved for Public Release; Distribution Unlimited

12b. DISTRIBUTION CODE

13. ABSTRACT ***(Maximum 200 words)***

Monocrystalline β(3C)-SiC films were grown on α(6H)-SiC(0001) substrates using gas-source MBE, silane and ethylene precursors and a temperature range of 1050-1450°C. Cubic (3C)-SiC was achieved at all T<1400°C; 6H-SiC films achieved at T>1400°C when H_2 diluent was present. The surface electronic states of clean 6H-SiC were investigated using ARUPS. Deposition and subsequent evaporation of Si and were used to clean the surface. LEED, AES and XPS showed that essentially all O and C contamination was removed. ARUPS revealed that all surfaces on the clean 6H-SiC except those terminated by H exhibited a degree of surface resonance (surfaces states) as a result of dangling bonds. H termination unpinned the surface Fermi level. NiAl contacts with a Ni passivating layers were deposited at room temperature on p-type 6H-SiC (0001) substrates. The as-deposited contacts were rectifying with very low leakage current densities (~1×10^{-8} A/cm² at 10 V), ideality factors between 1.4 and 2.4, and a Schottky barrier height (SBH) of approximately 1.37 eV. As-deposited Ni and Au contacts on p-type 6H-SiC displayed similar current-voltage characteristics with calculated SBH's of 1.31 and 1.27 eV, respectively. The former became ohmic on p^+ (1×10^{19} cm^{-3}) 6H-SiC (0001) after annealing for 10-80 s at 1000 °C in a N_2 ambient. The estimated specific contact resistivity from a non-mesa etched TLM pattern was $(2\text{-}3)\times10^{-2}$ Ω•cm². An AES depth profile obtained by of a film annealed for 80 s showed the formation of Al oxide at the surface. The Ni/NiAl contacts deposited on p-type SiC with lower carrier concentrations ($1\text{-}5\times10^{18}$ cm^{-3}) were not ohmic after annealing at 1000 °C for 10-60 s but became nearly ohmic after annealing for 80 s. MIS diodes (Al/AlN/α-SiC(0001)) have been fabricated with various thicknesses of AlN deposited using gas-source MBE. High frequency C-V measurements between 10 kHz and 1 MHz showed that thin layers (<1000Å) of AlN exhibited moderate leakage currents; thicker layers reduced this problem. The diodes could be accumulated and depleted over the entire frequency range studied. Inversion was not achieved at room temperature. A dependence of the dielectric constant on frequency was also observed.

14. SUBJECT TERMS

β-SiC, 6H-SiC, AlN, gas source molecular beam epitaxy, surface states, surface resonance, ohmic contacts, rectifying contacts, Ni/Al alloys, leakage current, Schottky barrier height, MIS diodes

15. NUMBER OF PAGES

30

16. PRICE CODE

17. SECURITY CLASSIFICATION OF REPORT	18. SECURITY CLASSIFICATION OF THIS PAGE	19. SECURITY CLASSIFICATION OF ABSTRACT	20. LIMITATION OF ABSTRACT
UNCLAS	UNCLAS	UNCLAS	SAR

I. Introduction

Silicon carbide (SiC) is a wide bandgap material that exhibits polytypism, a one-dimensional polymorphism arising from the various possible stacking sequences of the silicon and carbon layers. The lone cubic polytype, β-SiC, crystallizes in the zincblende structure and is commonly referred to as 3C-SiC. In addition, there are also approximately 250 other rhombohedral and hexagonal polytypes [1] that are all classed under the heading of α-SiC. The most common of the α-SiC polytypes is 6H-SiC, where the 6 refers to the number of Si/C bilayers along the closest packed direction in the unit cell and the H indicates that the crystal structure is hexagonal.

Beta (3C)-SiC is of considerable interest for electronic applications that utilize its attractive physical and electronic properties such as wide bandgap (2.2 eV at 300K) [2], high breakdown electric field (2.5×10^6 V/cm) [3], high thermal conductivity (3.9 W/cm °C) [4], high melting point (3103K at 30 atm) [5], high saturated drift velocity (2×10^7 m/s) [6], and small dielectric constant (9.7) [7]. Primarily due to its higher electron mobility than that of the hexagonal polytypes, such as 6H-SiC [8], β-SiC remains preferable to hexagonal SiC for most device applications.

Most 3C-SiC thin film growth to date has been performed on Si substrates. Large-area, crack-free, and relatively thick (up to 30 μm) epitaxial 3C-SiC thin films have been grown on Si (100) by exposing the Si substrate to a C-bearing gaseous species prior to further SiC growth [7, 9, 10]. However, these films exhibited large numbers of line and planar defects due to large lattice and thermal mismatches between SiC and Si. One particular type of planar defect, the inversion domain boundary (IDB), was eliminated with the use of Si (100) substrates cut 2°–4° toward [011] [11–13]. Growth on Si substrates has allowed much understanding of SiC growth processes and device development to occur, but the large thermal and lattice mismatches between SiC and Si hamper further development using Si substrates. As a result, great effort has been made to develop methods for growth SiC single crystal substrates for homoepitaxial growth of SiC thin films.

Since the 1950's, monocrystalline single crystals of 6H-SiC have been grown at using the Lely sublimation process [14]. However, nucleation was uncontrolled using this process and control of resultant polytypes was difficult. SiC single crystals inadvertently formed during the industrial Acheson process have also been used as substrates for SiC growth. However, neither these crystals or those formed using the Lely process are large enough for practical device applications. Recently, using a seeded sublimation-growth process, boules of single polytype 6H-SiC of > 1 inch diameter of much higher quality of that obtained using the Lely process have been grown. The use of single crystals of the 6H polytype cut from these boules has given a significant boost to SiC device development.

Silicon carbide epitaxial thin film growth on hexagonal SiC substrates has been reported since the 1960's. The use of nominally on-axis SiC substrates has usually resulted in growth of 3C-SiC films. Films of 3C-SiC (111) grown by CVD have been formed on 6H-SiC substrates less than 1° off (0001) [15]. Films of 3C-SiC on 6H-SiC substrates have typically had much lower defect densities than those grown on Si substrates. The major defects present in 3C-SiC/6H-SiC films have been double positioning boundaries (DPB) [16]. Despite the presence of DPBs, the resultant material was of sufficient quality to further device development of SiC. The use of off-axis 6H-SiC (0001) substrates has resulted in growth of high-quality monocrystalline 6H-SiC layers with very low defect densities [17].

In addition, the use of more advanced deposition techniques, such as molecular beam epitaxy (MBE), has been reported for SiC in order to reduce the growth temperature and from about 1400–1500°C on 6H-SiC substrates. Si and C electron-beam sources have been used to epitaxially deposit SiC on 6H-SiC (0001) at temperatures of 1150°C [18]. Ion-beam deposition of epitaxial 3C-SiC on 6H-SiC has also been obtained at the temperature of 750°C using mass-separated ion beams of $^{30}Si^{+}$ and $^{13}C^{+}$ [19].

Aluminum nitride (AlN) is also of particular interest at this time because of its very large bandgap. It is the only intermediate phase in the Al-N system and normally forms in the wurtzite (2H-AlN) structure. Most current uses of AlN center on its mechanical properties, such as high hardness (9 on Mohs scale), chemical stability, and decomposition temperature of about 2000°C [20]. Properties such as high electrical resistivity (typically $\geq 10^{13}$ Ω-cm), high thermal conductivity (3.2 W/cm K) [21], and low dielectric constant ($\varepsilon \approx 9.0$) make it useful as a potential substrate material for semiconductor devices as well as for heat sinks. The wurtzite form has a bandgap of 6.28 eV [22] and is a direct transition, thus it is of great interest for optoelectronic applications in the ultraviolet region.

Because of the difference in bandgaps (2.28 eV for 3C-SiC; 3.33 eV for 2H-SiC and 6.28 eV for 2H-AlN) between the materials, a considerable range of wide bandgap materials, made with these materials, should be possible. Two procedures for bandgap engineering are solid solutions and multilayers. A particularly important factor is that the two materials have a lattice mismatch of less than one percent.

Research in ceramic systems suggests that complete equilibrium solid solubility of AlN in SiC may exist, but only above ≈2000°C [23]. However, these solutions should be possible using the very non equilibrium technique of MBE. Solid solutions of the wurtzite crystal structure should have E_g from 3.33 eV to 6.28 eV at 0 K. Although it has not been measured, the bandgap of cubic AlN has been estimated to be around 5.11 eV at absolute zero and is believed to be indirect [24]. Cubic solid solutions should thus have E_g from 2.28 eV to roughly 5.11 eV at 0 K and would be indirect at all compositions if theory holds true.

Because of their similarity in structure and close lattice and thermal match, AlN-SiC heterostructures are feasible for electronic and optoelectronic devices in the blue and infrared region. Monocrystalline AlN layers have been formed by CVD on SiC substrates [25] and SiC layers have been formed on AlN substrates formed by AlN sputtering on single crystal W [26]. In addition, theory on electronic structure and bonding at SiC/AlN interfaces [24] exists and critical layer thicknesses for misfit dislocation formation have been calculated for cubic AlN/SiC [27]. Note that AlN (at least in the wurtzite structure) is a direct-gap material and SiC is an indirect gap material. Superlattices of these materials would have a different band structure than either constituent element. The Brillouin zone of a superlattice in the direction normal to the interfaces is reduced in size. This reduction in zone size relative to bulk semiconductors causes the superlattice bands to be "folded into" this new, smaller zone. This folding can cause certain superlattice states to occur at different points in k space than the corresponding bulk material states [28]. This can lead to direct transitions between materials which in the bulk form have indirect transitions. This has been demonstrated in the case of $GaAs_{0.4}P_{0.6}$/GaP and $GaAs_{0.2}P_{0.8}$/GaP superlattices, where both constituents are indirect in the bulk form [29]. Whether this is possible in the case of AlN/SiC is unknown, but very intriguing. It may be possible to obtain direct transitions throughout nearly the entire bandgap range with use of superlattices of AlN and SiC. Use of solid solutions in superlattices introduces additional degrees of freedom. For example, the bandgap can be varied independently of the lattice constant with proper choice of layer thickness and composition if superlattices of solid solutions of AlN and SiC were formed.

Due to the potential applications of solid solutions and superlattice structures of these two materials, an MBE/ALE system was commissioned, designed, and constructed for growth of the individual compounds of SiC and AlN, as well as solid solutions and heterostructures of these two materials. Chemical interdiffusion studies concerned with the kinetics and mechanisms of mass transport of Si, C, Al and N at the SiC/AlN interface are also being conducted in tandem with the deposition investigations.

A very important additional goal of this research is to understand what controls the contact electrical characteristics of specific metals to n-type and p-type 6H-SiC(0001) and to use this information to form good ohmic and Schottky contacts. Several metals and alloys have been and will be studied. The selection process began by taking the simplest case, an ideal contact which behaves according to Schottky-Mott theory. This theory proposes that when an intimate metal-semiconductor contact is made the Fermi levels align, creating an energy barrier equal to the difference between the work function of the metal and the electron affinity of the semiconductor. It is the height of this barrier which determines how the contact will behave; for ohmic contacts it is desirable to have either no barrier or a negative barrier to electron flow, while for a good Schottky contact a large barrier is desired.

Although the contact materials have been chosen optimistically, i.e. on the basis that they will form ideal contacts, some evidence exists that the contact properties will be more complicated. J. Pelletier *et al.* [30] have reported Fermi level pinning in 6H-SiC due to intrinsic surface states, suggesting little dependence of barrier height on the work function of the metal. In addition, L. J. Brillson [31, 32] predicts the pinning rate to be higher for more covalently bonded materials. Other complications may arise if the surface is not chemically pristine. A major part of this project is devoted to determining whether the contacts behave at all ideally, and if not, whether the Fermi level is pinned by intrinsic or extrinsic effects.

Along with examining the barriers of the pure metal contacts, the chemistry upon annealing is also being studied and correlated with the resulting electrical behavior. The electrical behavior is also quantified both macroscopically in terms of current-voltage characteristics and microscopically in terms of barrier height. The identification of the phases formed at the interface during deposition or subsequent annealing are determined using high resolution analytical TEM. Changes in the interface microstructure are also being correlated with the electrical characteristics of the contacts.

Within this reporting period, investigations concerned with (1) growth of monocrystalline epitaxial films of β(3C)-SiC(111) and α(6H)-SiC(0001) on vicinal (~3.5° off (0001) towards $<11\bar{2}0>$) α(6H)-SiC(0001) substrates via gas-source(GS) MBE, (2) the determination of surface states on non-hydrogen bonded surfaces of α(6H)-SiC(0001) previously cleaned via exposure to SiH_4 and the subsequent evaporation of Si, (3) the deposition and characterization of new ohmic and rectifying contacts to p-type 6H-SiC and (4) fabrication by GSMBE and electrical characterization of Al/AlN/SiC MIS diodes.

The experimental procedures, results, discussion of these results, conclusions and plans for future efforts for each of the topics noted above are presented in the following sections. Each of these sections is self-contained with its own figures, tables and references.

References

1. G. R. Fisher and P. Barnes, Philos. Mag. B **61**, 217 (1990).
2. H. P. Philipp and E. A. Taft, in Silicon Carbide, A High Temperature Semiconductor, edited by J. R. O'Connor and J. Smiltens (Pergamon, New York, 1960), p. 371.
3. W. von Muench and I. Pfaffender, J. Appl. Phys. **48**, 4831 (1977).
4. E. A. Bergemeister, W. von Muench, and E. Pettenpaul, J. Appl. Phys. **50**, 5790 (1974).
5. R. I. Skace and G. A. Slack, in Silicon Carbide, A High Temperature Semiconductor, edited by J. R. O'Connor and J. Smiltens (Pergamon, New York, 1960), p. 24.
6. W. von Muench and E. Pettenpaul, J. Appl. Phys. **48**, 4823 (1977).
7. S. Nishino, Y. Hazuki, H. Matsunami, and T. Tanaka, J. Electrochem Soc. **127**, 2674 (1980).
8. P. Das and K. Ferry, Solid State Electronics **19**, 851 (1976).
9. K. Sasaki, E. Sakuma, S. Misawa, S. Yoshida, and S. Gonda, Appl. Phys. Lett. **45**, 72 (1984).

10. P. Liaw and R. F. Davis, J. Electrochem. Soc. **132**, 642 (1985).
11. K. Shibahara, S. Nishino, and H. Matsunami, J. Cryst. Growth **78**, 538 (1986).
12. J. A. Powell, L. G. Matus, M. A. Kuczmarski, C. M. Chorey, T. T. Cheng, and P. Pirouz, Appl. Phys. Lett. **51**, 823 (1987).
13. H. S. Kong, Y. C. Wang, J. T. Glass, and R. F. Davis, J. Mater. Res **3**, 521 (1988).
14. J. A. Lely, Ber. Deut. Keram. Ges. **32**, 229 (1955).
15. H. S. Kong, J. T. Glass, and R. F. Davis, Appl. Phys. Lett. **49**, 1074 (1986).
16. H. S. Kong, B. L. Jiang, J. T. Glass, G. A. Rozgonyi, and K. L. More, J. Appl. Phys. **63**, 2645 (1988).
17. H. S. Kong, J. T. Glass, and R. F. Davis, J. Appl. Phys. **64**, 2672 (1988).
18. S. Kaneda, Y. Sakamoto, T. Mihara, and T. Tanaka, J. Cryst. Growth **81**, 536 (1987).
19. S. P. Withrow, K. L. More, R. A. Zuhr, and T. E. Haynes, Vacuum **39**, 1065 (1990).
20. C. F. Cline and J. S. Kahn, J. Electrochem. Soc, **110**, 773 (1963).
21. G. A. Slack, J. Phys. Chem. Solids **34**, 321 (1973).
22. W. M. Yim, E. J. Stofko, P. J. Zanzucci, J. I. Pankove, M. Ettenberg, and S. L. Gilbert, J. Appl. Phys. **44**, 292 (1973).
23. See, for example, R. Ruh and A. Zangvil, J. Am. Ceram. Soc. **65**, 260 (1982).
24. W. R. L. Lambrecht and B. Segall, Phys. Rev. B **43**, 7070 (1991).
25. T. L. Chu, D. W. Ing, and A. J. Norieka, Solid-State Electron. **10**, 1023 (1967).
26. R. F. Rutz and J. J. Cuomo, in Silicon Carbide-1973, ed. by R. C. Marshall, J. W. Faust, Jr., and C. E. Ryan, Univ. of South Carolina Press, Columbia, p. 72 (1974).
27. M. E. Sherwin and T. J. Drummond, J. Appl. Phys. **69**, 8423 (1991).
28. G. C. Osbourn, J. Vac. Sci. Technol. B **1**, 379 (1983).
29. P. L. Gourley, R. M. Biefeld, G. C. Osbourn, and I. J. Fritz, Proceedings of 1982 Int'l Symposium on GaAs and Related Compounds (Institute of Physics, Berkshire, 1983), p. 248.
30. J. Pelletier, D. Gervais, and C. Pomot, J. Appl. **55**, 994 (1984).
31. L. J. Brillson, Phys. Rev. B **18**, 2431 (1978).
32. L. J. Brillson, Surf. Sci. Rep. **2**, 123 (1982).

II. Homoepitaxial Growth of Silicon Carbide Polytypes by Gas-source Molecular Beam Epitaxy

A. Introduction

Silicon carbide (SiC) is a wide band gap material that exhibits polytypism, a one-dimensional polymorphism arising from the various possible stacking sequences of, e. g., the silicon and carbon layers along the directions of closest packing. There are approximately 250 SiC polytypes[1]. Included in these is one cubic polytype. This single cubic polytype, β-SiC, crystallizes in the zincblende structure, has a room temperature band gap of 2.3 eV, and is commonly referred to as 3C-SiC. (In the Ramsdell notation, the three (3) refers to the number of Si and C bilayers necessary to produce a unit cell and the C indicates its cubic symmetry.) The other rhombohedral and hexagonal polytypes are classed under the heading of α-SiC. The most common of these latter polytypes is 6H-SiC with a room temperature band gap of ≈ 3.0 eV.

Since the 1950's, monocrystalline single crystals of 6H-SiC have been grown at using the Lely sublimation process[2]. However, nucleation was uncontrolled using this process and control of resultant polytypes was difficult. SiC single crystals inadvertently formed during the industrial Acheson process have also been used as substrates for SiC growth. However, neither these nor those formed using the Lely process are large enough for practical device applications. Recently, using a seeded sublimation-growth process, boules of single polytype 6H-SiC of >1 inch diameter of much higher quality of that obtained using the Lely process have been grown. The use of single crystals of the 6H polytype cut from these boules has given a significant boost to SiC device development.

SiC epitaxial thin film growth on hexagonal SiC substrates has been reported since the 1960's. The use of nominally on-axis SiC substrates has usually resulted in growth of 3C-SiC films. Films of 3C-SiC(111) grown by CVD have been formed on 6H-SiC substrates less than 1° off (0001)[3]. Films of 3C-SiC on 6H-SiC substrates have typically had much lower defect densities than those grown on Si substrates. The major defects present in β-SiC/6H-SiC films have been double positioning boundaries (DPB)[4]. Despite the presence of DPBs, the resultant material was of sufficient quality to further device development of SiC. The use of off-axis 6H-SiC(0001) substrates has resulted in growth of high-quality monocrystalline 6H-SiC layers with very low defect densities[5].

In addition, the use of more advanced deposition techniques, such as molecular beam epitaxy (MBE), has been reported for SiC in order to reduce the growth temperature and from about 1400-1500 °C on 6H-SiC substrates. Si and C electron-beam sources have been used to epitaxially deposit SiC on 6H-SiC (0001) at temperatures of 1150 °C[6]. Previous reports by all investigators have documented 3C-SiC growth only on 6H-SiC(0001) by MBE.

B. Experimental Procedure

Thin, epitaxial films of SiC were grown on the Si-face of 6H-SiC(0001) substrates supplied by Cree Research, Inc. These vicinal 6H-SiC(0001) wafers, oriented 3-4° towards [11$\bar{2}$0], contained a 0.8 μm epitaxial 6H-SiC layer deposited via CVD and a thermally oxidized 75 nm layer to aid in wafer cleaning. A novel *in situ* cleaning procedure, described in previous reports, has been developed using reaction and desorption of the silicon-containing precursor (SiH_4). The surface preparation procedure involves cleaning with 10% HF and a 10 minute anneal at 1050 °C in UHV, as well as a silane exposure and boil-off. This additional cleaning step, intended to remove any residual oxygen, fluorine or other contaminants and create a silicon terminated surface, exposes the substrate to 0.1 sccm SiH_4 for 2 minutes at 1050 °C until the surface undergoes a reconstruction from the 1×1 to 3×3 as observed by RHEED. This 3×3 reconstruction is indicative of a Si-rich surface. (For a description of the various surface reconstructions of SiC, please refer to Kaplan[7].) The 3×3 reconstructed samples were annealed at 1200 °C for 10 minutes causing them to revert to the 1×1 pattern. At this point the films were grown.

All growth experiments were carried out in the gas-source molecular beam epitaxy system detailed in previous reports. The new heater assembly[8], designed for high temperature attainment, has been installed and operates as expected allowing for substrate temperatures as high as 1500 °C. The sources of Si and C were SiH_4 and C_2H_4 (both 99.99% pure), respectively. Flow ratios of SiH_4 and C_2H_4 were varied from 2:1 to 2:3. Hydrogen (99.9995% pure) was also introduced at 5.0 sccm into the reaction chamber during some depositions. Substrate temperatures were varied from 1050-1450 °C. Typical base pressures of 10^{-9} Torr were used. All experiments were performed for 2 hours on vicinal 6H-SiC(0001) substrates and examined by *in situ* reflection high-energy electron diffraction (RHEED) at the end of the growth run.

C. Results

Most prior growth conditions have resulted in monocrystalline, epitaxial layers of 3C-SiC with rough surfaces and the appearance of three-dimensional growth originating at the terraces of the vicinal substrates. The resulting films have been generally cubic and contain double positioning boundaries as evidenced by the RHEED and HRTEM. These results have been detailed in previous reports. Sporadic deposition of 6H-SiC has also been achieved and described previously; however, a clear understanding of the growth conditions necessary to grow 6H-SiC had not been determined.

When no hydrogen was present in the reaction chamber, films of SiC grown at all temperatures and gas flow ratios were cubic. Experiments conducted when hydrogen was introduced into the reaction chamber resulted in cubic films at substrate temperatures below

1400 °C and 6H-SiC films at temperatures above this temperature. Although all SiC films were monocrystalline by RHEED analysis for all conditions studied, 6H-SiC was only achieved at substrate temperatures ≥ 1400 °C under 5.0 sccm hydrogen flow. Figure 1 shows representative patterns. There were essentially three different RHEED patterns that were observed. Figures 1a and 1b are characteristic of cubic SiC patterns. Figure 1a is typical of films grown at temperatures below 1100 °C; Figure 1b, higher temperatures. Figure 1c is characteristic of a hexagonal (6H) pattern.

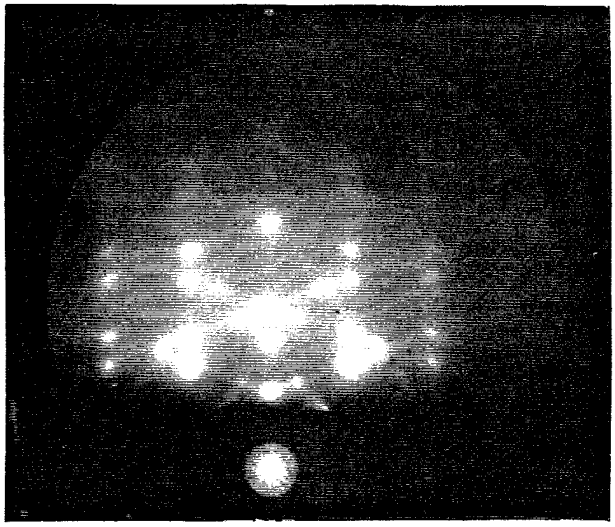

a)

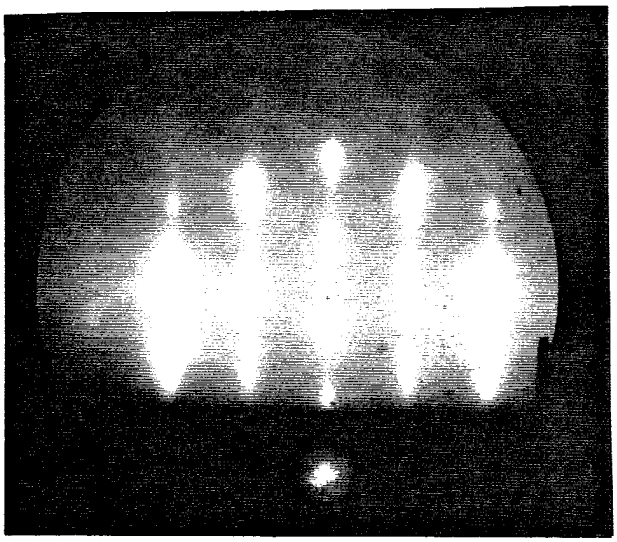

b)

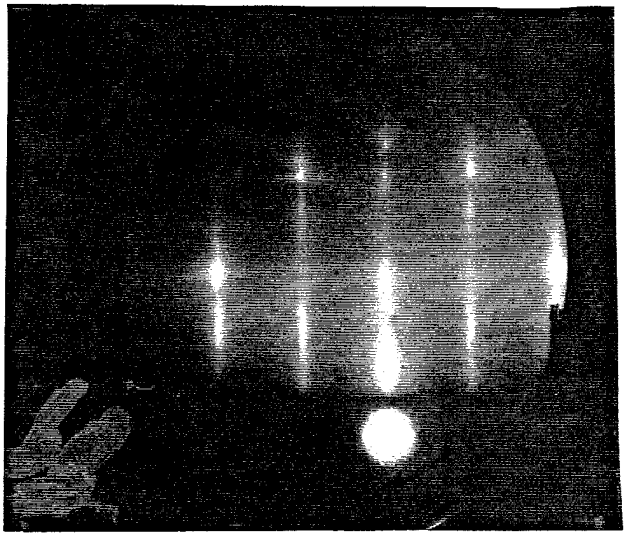

c)

Figure 1. RHEED photographs for a) growth runs below 1100 °C, b) growth runs above 1100°C and c) growth runs above 1400°C in flowing H_2.

D. Discussion

The use of hydrogen to produce homoepitaxial 6H-SiC is not a new technique. Hydrogen makes up the majority of the gas flow in CVD growth of SiC but has not been used previously in the MBE growth of SiC. The presence of hydrogen and the high temperatures of growth used here are necessary to achieve 6H-SiC films. It is expected that, at lower temperatures without the presence of atomic hydrogen, the decomposition of ethylene is incomplete without free silicon and, as a result, the films are a result of sporadic nucleation in locations where excess silicon species are present.

E. Conclusions

Preliminary studies into the growth conditions necessary to reproducibly achieve homoepitaxial 6H-SiC films have been performed. The initial results indicate that the most important factors in SiC polytype control (3C versus 6H) are the substrate temperature and the presence of hydrogen.

F. Future Research Plans and Goals

A study on both n- and p-type (with solid Al from a standard MBE effusion cell) is also underway. Further study of the effects of temperature, flow ratios and dopant incorporation are now being initiated.

G. References

1. G. R. Fisher and P. Barnes, Philos. Mag. B **61**, 217 (1990).
2. J. A. Lely, Ber. Deut. Keram. Ges. **32**, 229 (1955).
3. H. S. Kong, J. T. Glass, and R. F. Davis, Appl. Phys. Lett. **49**, 1074 (1986).
4. H. S. Kong, B. L. Jiang, J. T. Glass, G. A. Rozgonyi, and K. L. More, J. Appl. Phys. **63**, 2645 (1988).
5. H. S. Kong, J. T. Glass, and R. F. Davis, J. Appl. Phys. **64**, 2672 (1988).
6. S. Kaneda, Y. Sakamoto, T. Mihara, and T. Tanaka, J. Cryst. Growth **81**, 536 (1987).
7. R. Kaplan, Surface Sci. **215**, 111 (1989).
8. An invention disclosure explaining this heating element, made from SiC-coated graphite, has been submitted to the NCSU Technology Administration and Development Office.

III. Angular Resolved UPS (ARUPS) Investigation of 6H SiC Electronic Surface Structure

A. Introduction

The necessity for electronic devices with higher performance characteristics is ever increasing, and thus, surface cleaning without damage becomes especially important. Electronic performance is related to electronic structure, therefore, electronic structure as a function of the cleaning process must be examined. Because SiC tends to graphitize with annealing, a cleaning procedure which allows replacement of lost Si is desirable. R. Kaplan investigated this by annealing ß and 6H SiC samples in a silicon flux[1]. Hydrogen plasma processing has been demonstrated in cleaning silicon wafers[2]. The use of silane annealing (CVD cleaning) and a 1% silane/H_2 gas mixture has been discussed in a previous report[3]. This report focuses on the CVD cleaning process and characterization of the surface states.

UPS was used to examine the electronic states of the processed surface. Surface states, possibly caused by dangling bonds on a clean surface, were observed. Surface states appeared as distinctive features in the spectra. ARUPS was used to measure the dispersion of the surface momentum states. The surface state features of the spectra were sensitive to chemisorption of atoms or molecules to the surface[4]. Hydrogen termination was used in an attempt to further study Fermi level pinning by surface states[5].

B. Experimental Procedures

These studies were performed in an integrated ultra high vacuum transfer system. The details of the system have been presented elsewhere[6]. The capabilities included plasma processing, UPS, XPS, MBE, LEED and Auger electron spectroscopy (AES).

The sample used for this study was a 1 inch (25 mm) n-type SiC wafer. The wafer was the Si-terminated (0001) surface oriented 3-4° towards the [11$\bar{2}$0] surface. Tungsten was deposited on the back of the wafer to allow for uniform heating of the sample. Earlier work involved Pt as the backing material. This proved unsatisfactory as the Pt-C compounds formed were not stable at experimental temperatures. In one case, Pt appeared to diffuse through the sample. The *ex situ* preparation was a 10 minute dip in 10% HF solution.

For cleaning in the Gas Source Molecular Beam Epitaxy (GSMBE) system, the following procedures were used. Once in vacuum, the SiC crystals were inserted into the ALE system where they were outgassed at 250°C, 450°C, and 700°C for 30 minutes prior to any silane cleaning. All samples treated in this manner exhibited (1×1) LEED patterns. For CVD cleaning in the GSMBE, we exposed the sample to 1200 Langmuirs of silane for 15 minutes.

The plasma system has a base pressure of 1.0×10^{-9} Torr but operates in the milliTorr range of pressure. Hydrogen of up to 100 sccm can flow into the system. One may also flow, at a rate of 10 sccm, a mixture of 1% silane/H_2. Power is coupled into the chamber through rf

induction. Typical power rates are from 20 to 400 watts depending on the type of cleaning/etching desired. For CVD cleaning in the plasma chamber, 10 sccm of 1% SiH/H was used which gave a pressure of 25 mTorr. The annealing temperature was held at 825°C for 5 minutes. CVD cleaning in the plasma system was virtually identical to the GSMBE. However, the higher flux allows for quicker processing. Hydrogen termination was accomplished by 1 minute of flowing 86 sccm of H_2 (giving a pressure of 16 mTorr) with 20 Watts of power at a temperature of 450°C.

The UPS chamber had a base pressure of 2×10^{-10} Torr. Operating conditions involved pressures up to 1×10^{-9} Torr, but the higher pressure was due to the helium inflow and did not contaminate the sample. The UPS system utilized a helium resonance lamp (the He I line) to provide a source of 21.2 eV light. The ability existed to use the neon 16.8 eV emission line. This was useful for distinguishing between bulk and surface features. The bulk states will shift with respect to the Fermi level while surface features will not. Photoemitted electrons were measured with a 50 mm mean radius hemispherical electron analyzer operated at a 0.15 eV energy resolution and a 2° angular resolution. The analyzer (VSW HA50) is mounted on a double goniometer and can be tilted with respect to the sample in two independent directions. This capability was used to perform angular resolved UPS (ARUPS). Angles of up to 40° were examined for various reconstructions of the surface. The SiC samples were fastened by tantalum wire to a molybdenum sample holder. The sample holder was biased by up to 4 V to allow low energy electrons to overcome the work function of the analyzer. The Fermi level of the system (sample and analyzer) was determined by UPS measurement of the sample holder with no sample bias (i.e., grounded). The sample holder can be heated to 1150 °C.

The sample was examined in the case of the 3×3 reconstruction and the $\sqrt{3} \times \sqrt{3}$ R30° reconstruction as well as the 1×1 case. In some cases annealing was required to obtain the 1×1 surface and was always necessary to obtain the $\sqrt{3} \times \sqrt{3}$.

C. Results

The surface was cleaned by an *ex situ* 10% HF dip for 10 minutes to remove thick oxide. This was followed by annealing the sample in a silane flux. The silane flow was 10 sccm of 1% SiH_4/H_2 for 5 minutes while a temperature of 825°C was maintained. AES of this process, along with the LEED pattern, is shown in Fig. 1 and compared to an *ex situ* clean alone. These parameters resulted in substantial removal of oxygen and surface hydrocarbons. The CVD clean resulted in a 3×3 reconstruction, possibly due to a silicon adatom structure, indicating a Si rich surface.[7]

The CVD clean removed substantial amounts of oxygen and hydrocarbons. This produced an ordered surface with a 3×3 reconstruction. From the Auger spectra, a Si/C ratio of 1.8

indicating a silicon rich surface was determined. The LEED pattern was attributed to a Si adatom structure. The 1×1 LEED pattern seemed to occur for a wide range of Si/C ratios. The $\sqrt{3} \times \sqrt{3}$ surface arose from annealing the 1×1 and was shown by Auger to be Si deficient.

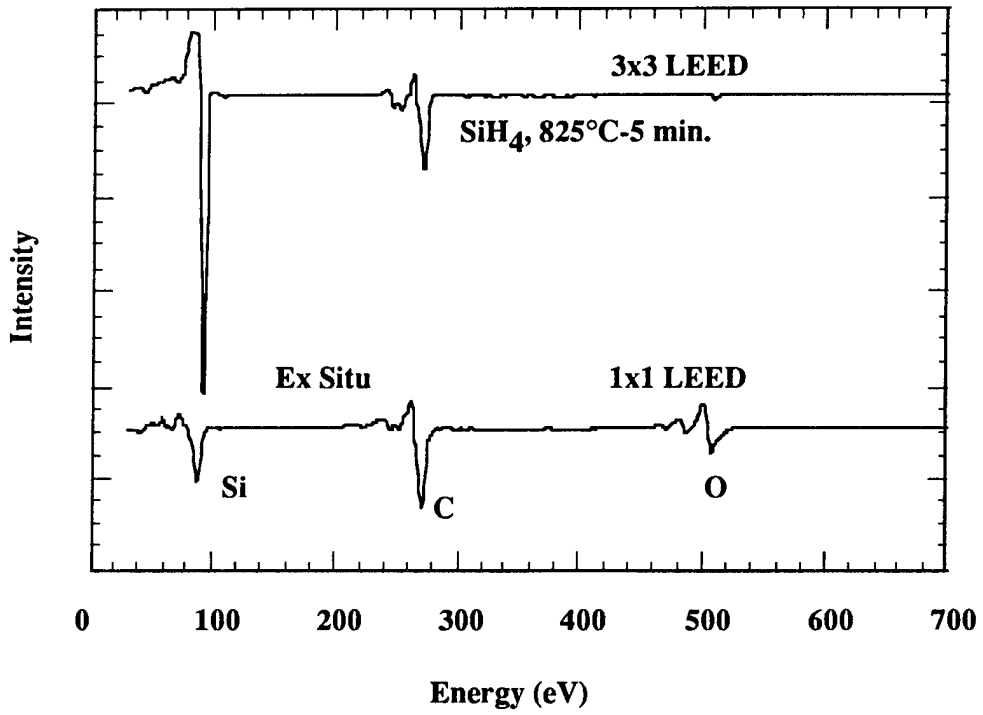

Figure 1. Silane CVD clean of 6H SiC.

ARUPS scans were performed on the CVD cleaned sample, a reconstructed sample, the unreconstructed 1×1 surface and a hydrogen terminated clean sample. The $\sqrt{3} \times \sqrt{3}$ R30° surface was prepared by annealing to 960 °C without a silane flow and was silicon deficient. The hydrogen terminated surface was a CVD cleaned sample which had a LEED pattern of 1×1. It was exposed to a hydrogen plasma to investigate the role of dangling bonds in the UPS spectra. The UPS data for the three main surfaces appear in Fig. 2.

The angular dispersion of the 3×3 surface is shown as a representative spectra for the dispersion studies, see Fig. 3.

The UPS investigation yielded very interesting results. Features in the spectra were seen which may be surface states. Note that the substrate is n type, yet in all cases emission started near the Fermi level; this suggested Fermi level pinning. Surface states were distinguishable from those of the bulk by using light of a different energy, as discussed above. To test the origin of the state, the plasma system was used to terminate the surface with hydrogen. As seen in Fig. 4, this resulted in the partial removal of the feature and a shift of the spectra away from the Fermi level. This change was attributable to the passivation of the surface. The dangling

bonds were satisfied by the hydrogen atoms which terminated the surface. Without the H termination, Fermi level pinning was achieved.

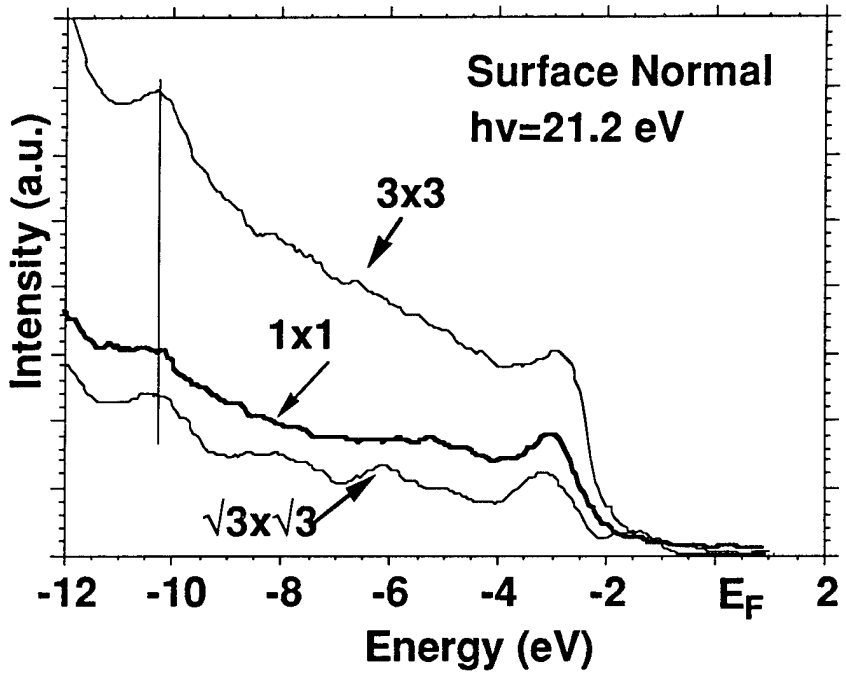

Figure 2. SiC electronic structure.

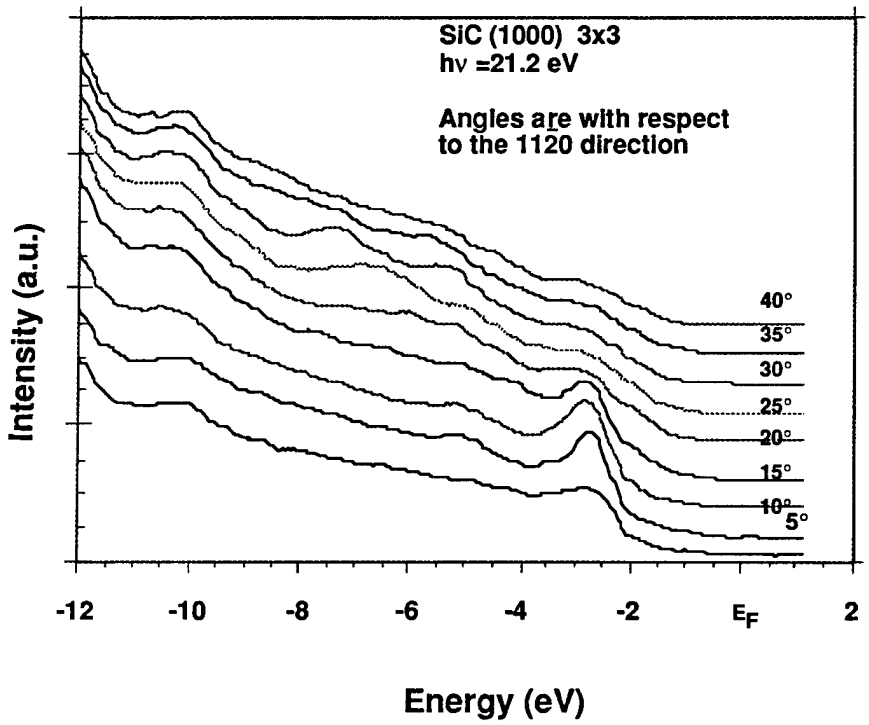

Figure 3. Angular dispersion of the 3×3 SiC surface.

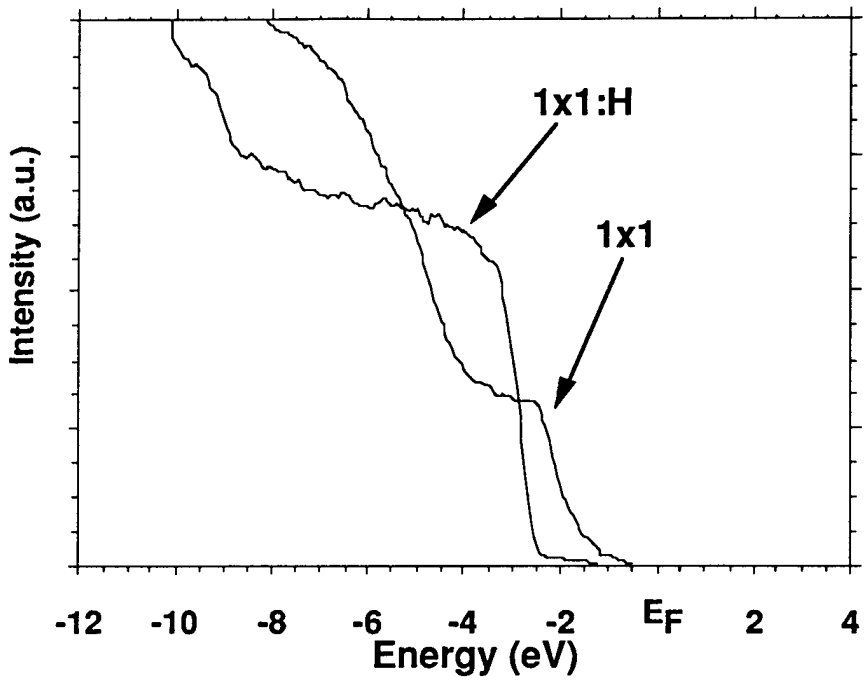

Figure 4. H termination unpins the Fermi level.

D. Discussion

Removing oxide and other contaminants from the surface allowed features in the spectra which were attributed to surface states in the electronic structure to be seen. These surface states were due to either dangling bonds on the surface or possibly back bonds to the C underlayer. The $\sqrt{3} \times \sqrt{3}$ surface appeared to have the most structure. The 1×1 surface, as mentioned previously, did not seem to be a unique surface, i.e. different stoichiometry gives the same 1×1 LEED pattern.

The effect of hydrogen termination confirmed that the UPS features were due to surface states. XPS confirmed the shift in spectra and was followed by Thermal Programmed Desorption (TPD) which showed large amounts hydrogen desorption. After this treatment, the shift was removed.

The usefulness of ARUPS allows mapping of the dispersion of the k states parallel to the surface. A discussion of this can be found in Uhrberg and Hannson's review [4]. The relation between the energy and the momentum states is given by

$$k_{\parallel} = \sin\theta e \sqrt{2mE_{Kin}/\mathrm{h}^2}$$

where θ_e is the angle of emission with 0 degrees as normal emission and E_{kin} is the kinetic energy of the photoemitted electrons. Using this relation, the dispersion as a function of wavevector was plotted, see Fig. 5.

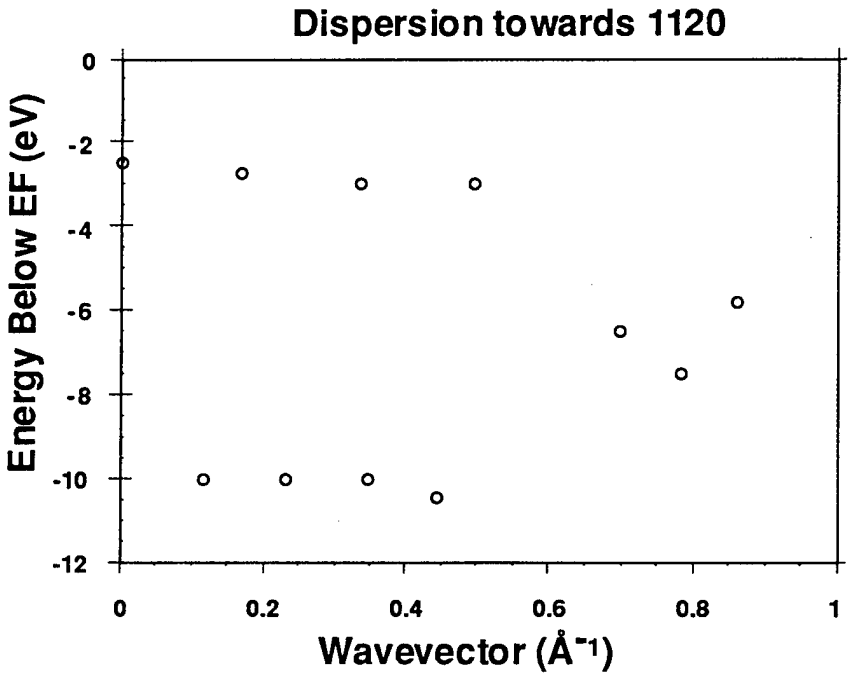

Figure 5. Wavevector dispersion.

E. Conclusions

Cleaning was demonstrated of 6H vicinal SiC substrates by silane CVD methods which have improved the pure chemical etch method. Substantial removal of surface hydrocarbons and oxides was shown. The 1×1 LEED pattern was not a good indicator of the surface cleanliness and, given the range of stoichiometries exhibited, it was not a useful indicator of surface condition.

The observation of surface states on SiC was made. All of the surfaces (except the hydrogen terminated) exhibited some degree of surface resonance (surface state). The $\sqrt{3} \times \sqrt{3}$ surface showed the most structure. This might be due to a higher number of dangling bonds per area. The hydrogen termination of the surface unpins the Fermi level. This was confirmed by both UPS and XPS. The removal of termination and the subsequent return of surface state features further strengthen the argument for dangling bonds as the cause of the surface features.

F. Future Plans

Further investigation of the surface state structure will be made by UPS. The surface has sufficient study to include metal overlayers and to begin ARUPS studies of Schottky barriers

on 6H SiC. This probe of the surface structure should lead to a better understanding of surface kinetics which in turn should help further develop the contact and heterojunction processes. An additional metallization chamber which has come on line will speed this research thrust as more metals will be available at the same time.

A chamber for HF vapor phase cleaning is in development for addition to the integrated transfer system. This will present an opportunity to investigate this mode of processing.

G. Acknowledgments

This work was supported in part by the Office of Naval Research through grants N0014-92-J-1477 and N0014-92-J-1604. The SiC substrates used were supplied by Cree Research. S. W. King provided XPS and the GS-MBE work. J. P. Barnak provided assistance with the plasma chamber as well as discussion. R. S. Kern was a valuable source of information.

H. References

1. R. Kaplan, Surface Science **215**, 111 (1989)
2. R. A. Rudder, S. V. Hattangady, J. B. Posthill, and R. J. Markunas, Mat. Res. Soc. Symp. **116**, 529 (1988)
3. ONR Semiannual Technical Report December 1994
4. R. I. G. Uhrberg , G. V. Hansson, Critical Reviews in Solid State and Materials Sciences, **17** (2) 136 (1991)
5. J. Pelletier, D. Gervais, and C. Pomot, J. Appl. Phys. **55**, 994 (1994)
6. J. van der Weide, R. J. Nemanich, J. Vac. Sci. Technol. B **10** 1940 (1992)
7. R. Kaplan

IV. Rectifying and Ohmic Contacts for P-Type Alpha (6H) Silicon Carbide

A. Introduction

The formation of low resistivity and thermally stable ohmic contacts to 6H-SiC remains a serious problem in the development of SiC device technology. For SiC power devices to have the advantage over Si, the contact resistivities must be below 1×10^{-5} Ω-cm^2 [1]. In addition, the electrical characterization of state-of-the-art SiC films depends on the ability to fabricate ohmic contacts on material with low carrier concentrations. Therefore, better ohmic contacts are needed both for improving device performance and for improving the quality of films which can be grown. The thermal stability of ohmic contacts is of particular concern for p-type SiC, which have traditionally relied on Al or Al alloys to dope the SiC surface below the contacts. While the fabrication of ohmic contacts to SiC also has usually depended on very heavily-doped surfaces, the introduction of high levels of dopants in the near surface device region of the epilayer prior to the deposition of the contact or by ion implantation through the contact makes probable the introduction of point and line defects as a result of the induced strain in the lattice. Based on all of these issues and experiments already performed at NCSU, our goals are to produce contacts which are thermally stable and have low contact resistivities while also reducing the need for doping by ion implantation.

Low resistance contacts to p-type SiC remain a substantial challenge for high temperature and high-power devices. An Al-Ti alloy [2] annealed at 1000°C for 5 min. was reported to yield contact resistances ranging from 2.9×10^{-2} Ω cm^2 for a carrier concentration of 5×10^{15} cm^{-3} to 1.5×10^{-5} Ω cm^2 for 2×10^{19} cm^{-3}. The thermal stability of these contacts was not reported. Aluminum deposited on a heavily-doped 3C-SiC interlayer on a 6H-SiC substrate and subsequently annealed at 950°C for 2 min. reportedly yielded contact resistivities of $2–3\times10^{-5}$ Ω cm^2 [3]. Because of its low melting point (660°C), however, pure Al would be unsuitable for high temperature applications. Platinum contacts annealed from 450 to 750°C in 100°C increments were also used as ohmic contacts to p-type SiC [4]. These contacts, which rely on the combination of a highly-doped surface and the high work function of Pt, have not been known to yield contact resistivities as low as those for the contacts containing Al.

Because Ni forms stable silicides but not carbides, it has the potential to draw Si out of the lattice, allowing Al to diffuse into the SiC and occupy Si sites. In contrast, Ti forms a very stable carbide [5] in addition to silicides and therefore readily competes for the C in TiAl contacts. This report describes electrical characteristics and chemical profile results of as-deposited NiAl Schottky contacts and NiAl ohmic contacts annealed at 1000 °C (10 to 80 s) on p-type 6H-SiC (0001). Future experiments with these contacts are also discussed along with other contact schemes which do not incorporate Al.

B. Experimental Procedure

Vicinal, single-crystal 6H-SiC (0001) wafers provided by Cree Research, Inc. were used as substrates in the present research. The wafers were doped with N or Al during growth to create n- or p-type material, respectively, with carrier concentrations of $1–5\times10^{18}$ cm^{-3}. Homoepitaxial layers (1–5 μm thick) grown by chemical vapor deposition (CVD) were Al-doped with carrier concentrations ranging from 1×10^{16} to 1×10^{19} cm^{-3}. The surfaces were oxidized to a thickness of 500–1000 Å in dry oxygen. The substrates were simultaneously cleaned and the oxide layer etched from the surface using a 10 min. dip in 10% hydrofluoric acid, transferred into the vacuum system, and thermally desorbed at 700 °C for 15 min. to remove any residual hydrocarbon contamination.

A UHV electron beam evaporation system was used to deposit the NiAl and Ni films. After depositing 1000 Å of NiAl, 500–1000 Å of Ni was deposited as a passivating layer. Pure Ni (99.99%) and pure Al (99.999%) pellets were arc melted to form alloyed pellets of 50:50 atomic concentration for evaporation of NiAl. The films were deposited onto unheated substrates at a rate of 10–20 Å/s. The pressure during the depositions was between 5×10^{-9} and 5×10^{-8} Torr.

Circular contacts of 500 μm diameter were fabricated for electrical characterization by depositing the metal films through a Mo mask in contact with the substrate. Silver paste served as the large area back contact. For contact resistance measurements, TLM patterns [6] were fabricated by photolithography. The Ni/NiAl films were etched in phosphoric acid : acetic acid : nitric acid (12 : 2 : 3) at 50 °C (etch rate ≈ 30 Å/s). The contact pads were 300×60 μm with spacings of 5, 10, 20, 30 and 50 μm. Mesas in the substrate were not fabricated. All subsequent annealing was conducted in a N_2 ambient in a rapid annealing furnace.

Electrical characteristics were obtained from current-voltage and capacitance-voltage measurements. Current-voltage (I-V) measurements were obtained with a Rucker & Kolls Model 260 probe station in tandem with an HP 4145A Semiconductor Parameter Analyzer. Capacitance-voltage (C-V) measurements were taken with a Keithley 590 CV Analyzer using a measurement frequency of 1 MHz.

Auger electron spectroscopy (AES) was performed with a JEOL JAMP-30 scanning Auger microprobe. The films were sputtered with Ar ions at a beam current and voltage of 0.3 μA and 3 kV, respectively, to obtain composition profiles through the thickness of the films.

C. Results

Chemical Characterization of As-deposited Films. The composition of the NiAl films deposited at room temperature were analyzed with AES. The first films deposited were found to contain approximately 3 at. % O. This contamination was attributed to O found in the Ni source. Alloyed pellets were subsequently fabricated using a new Ni source (99.99%).

An Auger depth profile of a film deposited from the latter source is shown in Fig. 1. While there was some modulation of the intensities, the overall composition remained relatively stable. The relative intensities of Ni and Al calculated from pure Ni and pure Al standards and their corresponding sensitivity factors are shown in Fig. 2. The average atomic composition was approximately 50:50.

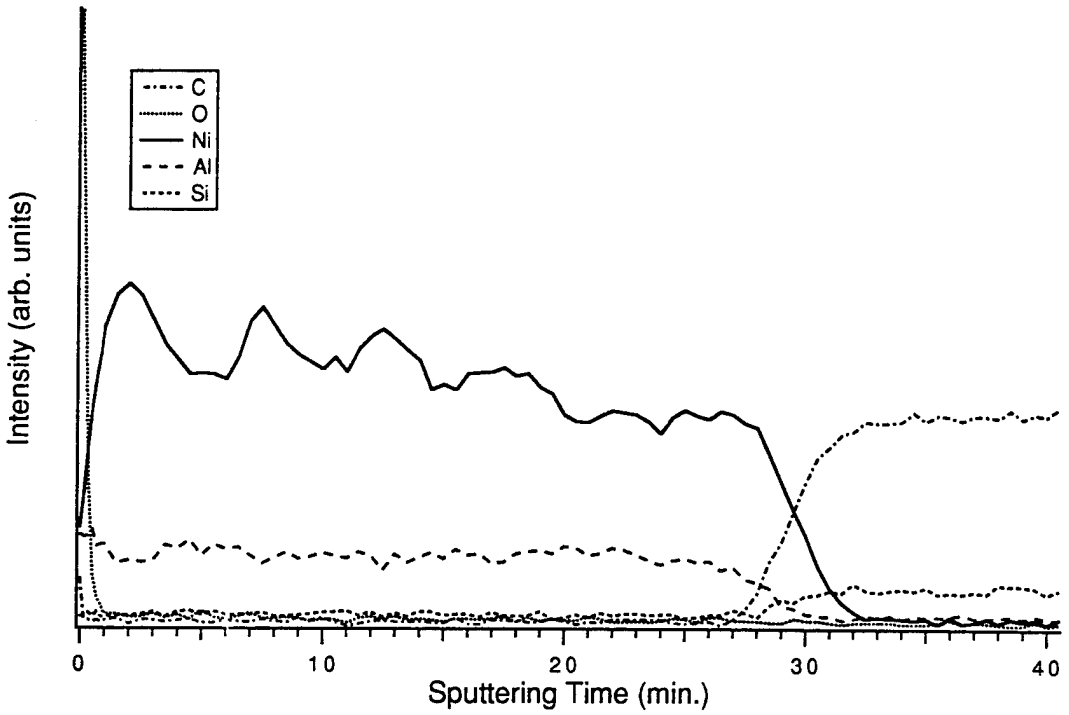

Figure 1. AES composition profile of 1000 Å of NiAl deposited at room temperature on (0001) 6H-SiC.

Schottky contacts. In the as-deposited condition the Ni/NiAl contacts were rectifying on p-type SiC with carrier concentrations of 1.6×10^{16} and 3.8×10^{18} cm^{-3} in the epilayer. The sample with the lower carrier concentration displayed leakage current densities of $\sim1\times10^{-8}$ A/cm^2 at 10 V and ideality factors between 1.4 and 2.4, while the latter sample displayed approximately five orders of magnitude higher leakage current densities and similar ideality factors. The average Schottky barrier heights (SBH's) calculated for the samples with the lower and higher carrier concentrations were 1.37 and 1.26 eV, respectively. The lower SBH calculated for the former sample is likely due to enhanced thermionic field emission through the upper energy region of the barrier because of the narrower depletion region. Hence, the 1.37 eV value is believed to be more accurate.

Similar results were obtained for as-deposited Ni and Au contacts on p-type ($2.1–4.5\times10^{16}$ cm^{-3}) 6H-SiC (0001). These samples displayed similar leakage currents and ideality factors of

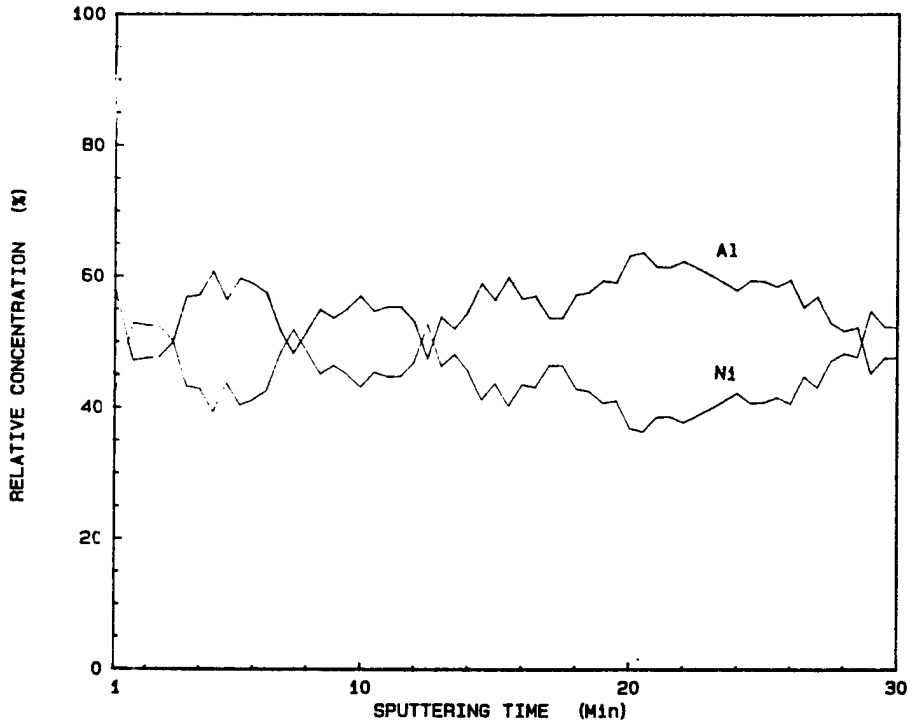

Figure 2. Relative concentrations of Ni and Al in the film represented in Fig. 1. The calculations were based on the signals from pure Ni and pure Al and their corresponding sensitivity factors.

1.3–2.1 and <1.1, respectively. From these measurements SBH's of 1.31 eV for the Ni contacts and 1.27 eV for the Au contacts were calculated. In comparison, as-deposited Ni on n-type (4.1×10^{16} cm^{-3}) 6H-SiC (0001) yielded ideality factors below 1.1, similar leakage current densities to those stated above, and SBH's of 1.14 eV and 1.21 eV calculated from I-V and C-V measurements, respectively.

Our measurements on p-type SiC have shown consistent differences from measurements on n-type 6H-SiC. The SBH's tended to be higher on p-type than on n-type material. While leakage currents for Au, NiAl, and Ni contacts on p-type 6H-SiC were comparable to Ni contacts on n-type 6H-SiC, the ideality factors were higher on p-type SiC. The higher ideality factors for contacts on p-type SiC indicate that thermionic emission was not the dominant current transport mechanism. In the future we may investigate these contacts with deep level transient spectroscopy (DLTS) to determine whether recombination at deep levels accounts for the different electrical behavior of the contacts on p-type material.

Ohmic Contacts. The Ni/NiAl contacts were sequentially annealed for total times of 10–80 s at 1000 °C in a N_2 ambient. This temperature was used because (1) limited intermixing of Al and SiC was reported at 900 °C [7] and (2) other papers report annealing in this temperature range for Al-based ohmic contacts on p-type SiC [2, 3, 8]. Because of the extremely high thermodynamic driving force for Al to form an insulating oxide layer

(ΔG_f (Al_2O_3) ~ -1300 kJ/mol at 1000 °C [JANAF - Chase, M., et al., JANAF Thermochem. Tables, 3d Ed. J. Phys. Chem. Ref. Data, 1985. 14(Supp. 1)]), 1000 Å of Ni was deposited on top of the NiAl contacts to slow the oxidation process.

Table I summarizes the results of I-V measurements taken at selected intervals through the annealing series for three samples with various carrier concentrations in the SiC epitaxial layer (1.4×10^{18}, 5.7×10^{18}, and 1.5×10^{19} cm^{-3}). The two samples with the lower carrier concentrations were not truly ohmic but became ohmic-like after annealing for 80 s. This annealing series will be continued to determine whether ohmic behavior in these two samples will ensue; however, the additional force on the probes needed to obtain consistent results indicates that an oxide has begun to form at the surface and may cause problems with further annealing. The sample with the higher carrier concentration was ohmic after annealing for 10 s. The calculated specific contact resistivity remained approximately 2.0×10^{-2} Ω cm^2 through annealing for 60 s. A slight increase to 3.1×10^{-2} Ω cm^2 was calculated after annealing for 80 s. This increase is believed to be due to the surface oxide layer. These values of specific contact resistivity should only be considered as preliminary estimates since only one level of the TLM measurement pattern was used. In the near future we plan to employ a circular TLM measurement structure [9], which consists of only one level and does not involve etching of the substrate.

Table I. Estimated specific contact resistivities / electrical behavior of Ni (1000 Å) / NiAl (1000 Å) / p-SiC after annealing at 1000 °C for 20, 40, 60, and 80 s for three samples with the carrier concentrations indicated. The specific contact resistivities were calculated from non-mesa etched linear TLM patterns.

Annealing Time	20 s	40 s	60 s	80 s
1.4×10^{18} cm^{-3}	non-ohmic	non-ohmic	non-ohmic	almost ohmic
5.7×10^{18} cm^{-3}	non-ohmic	non-ohmic	non-ohmic	almost ohmic
1.5×10^{19} cm^{-3}	2.0×10^{-2} Ω cm^2	1.9×10^{-2} Ω cm^2	2.2×10^{-2} Ω cm^2	3.1×10^{-2} Ω cm^2

D. Discussion

An Auger depth profile (Fig. 3) of Ni/NiAl/SiC annealed at 1000 °C for 80 s shows that the surface oxide is thicker than that on the as-deposited sample (Fig. 1). After sputtering for a couple of minutes, the O concentration dropped to below detectable limits; however, the data shows a decreasing Al concentration in the direction toward the SiC interface. This indicates

that the kinetics are more favorable for the Al to diffuse toward the surface and react with O than for the Al to react with the SiC. Some of the Ni has probably reacted with Si at the interface to form a silicide, as indicated by the local maximum in the Ni intensity near the SiC interface, while the peak in the C intensity indicates the presence of an adjacent C-rich layer.

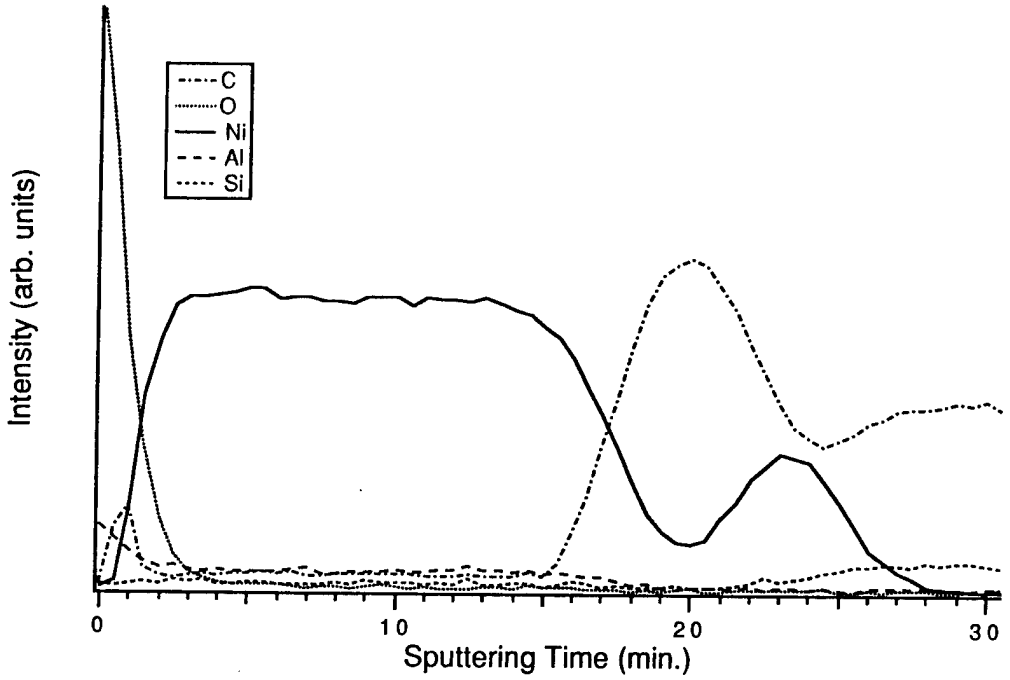

Figure 3. AES composition profile of Ni (1000 Å) / NiAl (1000 Å) / 6H-SiC annealed at 1000 °C for 80 s in N_2.

The demonstrated oxidation problem with Al necessitates the development of ohmic contacts which do not consist of substantial concentrations of Al. The following section discusses future plans for finishing the experiments on NiAl contacts and for initiating experiments on novel contact materials.

E. Conclusions

Nickel-aluminum was investigated primarily as an ohmic contact for p-type 6H-SiC because of the p-type doping of Al in SiC, the high melting point of NiAl (as compared to Al), and the tendency of Ni to form silicides but not carbides. This latter property potentially could have resulted in extraction of Si from the SiC lattice in exchange for Al, thereby enhancing the p-type carrier concentration at the surface. Although the I-V measurements indicate that some Al may be diffusing into the SiC after the longest annealing time performed (80 s at 1000 °C), this potential for reaction between Al and SiC appears to be exceeded by the driving force for

Al to diffuse to the surface and react with O. A concentration profile obtained from AES analysis shows that Al has diffused through the 1000 Å Ni overlayer to form a thin (200 Å estimated) oxide layer.

In addition to the ohmic behavior resulting from annealing the NiAl contacts, as-deposited Ni, NiAl, and Au contacts deposited at room temperature on p-type ($N_A < 5\times10^{16}$ cm^{-3}) 6H-SiC (0001) were rectifying with low leakage currents, ideality factors between 1.3 and 2.4, and SBH's of 1.31, 1.27, and 1.37 eV, respectively. These SBH's are higher than typically calculated for contacts on n-type 6H-SiC, as represented by the 1.14 eV value for Ni on n-type 6H-SiC and calculated from I-V measurements. A technique such as DLTS be used to explain the different behavior between Schottky contacts on n- and p-type SiC.

F. Future Research Plans and Goals

To complete our study on NiAl ohmic contacts for p-type SiC, the annealing series at 1000 °C will be extended. In addition, the specific contact resistivities will be remeasured using circular TLM patterns. This method consists of only one photolithographic level and should be more accurate than the single level, linear TLM patterns used for the calculations in this report. A photolithography mask with the circular TLM patterns is currently being designed and will be used in future research on ohmic contacts.

An alternate planned approach to Al-based ohmic contacts for p-type SiC will incorporate p-type semiconducting interlayers. The goal of this approach is to find a semiconducting material with a favorable band lineup with SiC (i.e., reduce the band bending) and to which an ohmic contact can easily be made. We have chosen to examine the $In_xGa_{1-x}N$ system for interlayer materials because of the lower density of surface states (and hence less band bending) and the range of band gaps over the composition range. We plan to measure the valence band offsets and electrical characteristics between various compositions of $In_xGa_{1-x}N$ (starting with x=0) and SiC. If a low energy barrier at the interface results, metals will be investigated for ohmic contacts for the interlayer / SiC structure.

G. References

1. D. Alok, B. J. Baliga, and P. K. McLarty, IEDM Technical Digest, IEDM 1993, 691 (1993).
2. J. Crofton, P. A. Barnes, J. R. Williams, and J. A. Edmond, Appl. Phys. Lett. **62**(4), 384 (1993).
3. V. A. Dmitriev, K. Irvine, and M. Spencer, Appl. Phys. Lett. **64**(3), 318 (1994).
4. R. C. Glass, J. W. Palmour, R. F. Davis, and L. S. Porter, U.S Patent No. 5,323,022 (1994).
5. J. L. Murray, Ed. Phase Diagrams of Binary Titanium Alloys (ASM International, Metals Park, Ohio, 1987).
6. H. H. Berger, Solid State Electronics **15**(2), 145 (1972).
7. V. M. Bermudez, J. Appl. Phys. **63**(10), 4951 (1988).

8. T. Nakata, K. Koga, Y. Matsushita, Y. Ueda, and T. Niina, in Amorphous and Crystalline Silicon Carbide and Related Materials II, M. M. Rahman, C. Y.-W. Yang, and G. L. Harris, Eds., Vol. 43 (Springer-Verlag, Berlin, 1989).
9. G. K. Reeves, Solid State Electronics **21**, 801 (1978).

V. Fabrication and Characterization of MIS Diodes of Al/AlN/SiC by Gas-Source Molecular Beam Epitaxy

A. Introduction

Silicon carbide (SiC) is a wide band gap material that makes it attractive for the fabrication of electronic devices that operate in a variety of harsh environments. SiC has a wide band gap (≈3.0 eV at room temperature), excellent thermal stability[1-3], a high thermal conductivity (4.9 W $cm^{-1}K^{-1}$)[4], a high breakdown field (2×10^6 V cm^{-1})[2] and a high saturated electron drift velocity (2×10^7 cm s^{-1})[3]. In the last few years, blue light emitting diodes (LEDs), junction field effect transistors (JFETs) and metal-oxide-semiconductor field effect transistors (MOSFETs) have become commercially available. Excellent reviews of these devices have been published[5-11].

Since metal-insulator-semiconductors (MIS) structures are an important part of today's microelectronics industry, MIS diodes (using SiO_2, in particular, as the insulator) have been studied by a number of researchers. The majority of the studies have been done on 6H-SiC substrates. Although some work[12-16] has also been done on 3C-SiC, the defective nature of the material make most of the measurements difficult to interpret since the resulting interface state densities and fixed oxide charge densities were very high. Most of this work has centered around the optimization of the oxidation both kinetically and electrically; however, the chemical character of the oxide has also been studied by Auger electron spectroscopy[17, 18] and secondary ion mass spectroscopy[16, 19, 20]. Nearly all reports (see for example[21]) report that the MOS diodes can be easily accumulated and depleted at room temperature; however, inversion can only be obtained when the samples are illuminated by a UV light. The lowest reported values[22] of fixed charge densities and interface state densities are 9×10^{11} cm^{-2} and 1.5×10^{11} cm^{-2} eV^{-1}, respectively. To date, there has only been one report[23] of a MIS diode made with an insulator other than SiO_2. In this case, Si_3N_4 was used, but had only minimal success due to very large density of defects and large leakage currents.

Aluminum nitride possesses a direct band gap of 6.28 eV at 300 K[24], a melting point in excess of 2275 K[25] and a thermal conductivity of 3.2 W cm^{-1} K^{-1}[26] As such, it is a candidate material for high-power and high-temperature microelectronic and optoelectronic applications with the latter employment being particularly important in the ultraviolet region of the spectrum[24]. These properties strongly indicate that superior surface acoustic wave devices, operational in aggressive media and under extreme conditions both as sensors for high temperatures and pressures and as acousto-optic devices can be developed[27-29]. However, progress regarding these (and other) applications is hampered by the lack of good single crystal material.

B. Experimental Procedure

Thin, epitaxial films of several thicknesses of AlN were grown on a variety of Si-face α-SiC(0001) substrates supplied by Cree Research, Inc. The different α-SiC(0001) wafers are listed in Table I. Each of the wafers contained a 0.8 μm epitaxial SiC layer deposited via CVD and a thermally oxidized 75 nm layer to aid in wafer cleaning. The surfaces were prepared by a 10% HF dip and a 10 minute anneal at 1050 °C in UHV as well as a silane exposure and boil-off described in previous reports.

Table I. SiC Substrates used in this Research

on-axis, n-type ($n = 2.8 \times 10^{16}$ cm^{-3}) 6H-SiC
off-axis, n-type ($n = 2.4 \times 10^{16}$ cm^{-3}) 6H-SiC
off-axis, p-type ($n = 2.1 \times 10^{16}$ cm^{-3}) 6H-SiC
off-axis, n-type ($n = 5.0 \times 10^{15}$ cm^{-3}) 4H-SiC

All growth experiments were carried out in the gas-source molecular beam epitaxy system detailed in previous reports. Films of AlN were grown at 1100 °C. Source were aluminum (99.9999% purity), evaporated from a standard MBE effusion cell operated in all cases at 1150°C, and 7.0 sccm ammonia (99.999% pure). Typical base pressures of 10^{-9} Torr were used. Aluminum contacts (area = 5×10^{-3} cm^2) were deposited on the AlN by means of a standard evaporator and In-Sn solder was used a contact to the SiC.

High frequency capacitance-voltage measurements were performed on a HP 4275A C-V analyzer and the quasistatic C-V and I-V measurements were performed on a HP 4140B analyzer. Measurements were performed with the assistance of S. Cohen of IBM T. J. Watson Research Center in Yorktown Heights, NY. These analyzers were programmed to measure C-V and I-V characteristics of the diodes as well as to calculate the insulator thickness from the capacitance. Measurements were performed on diodes with AlN thicknesses of 1000 Å and 2500 Å.

C. Results

In all cases, the diodes could be accumulated and depleted with the application of small gate voltages. Figure 1 shows C-V curves for a typical 1000 Å sample. However, deep depletion and inversion were not achieved in any case. For the 1000 Å samples, the leakage current was too high to accurately measure quasistatic C-V response.

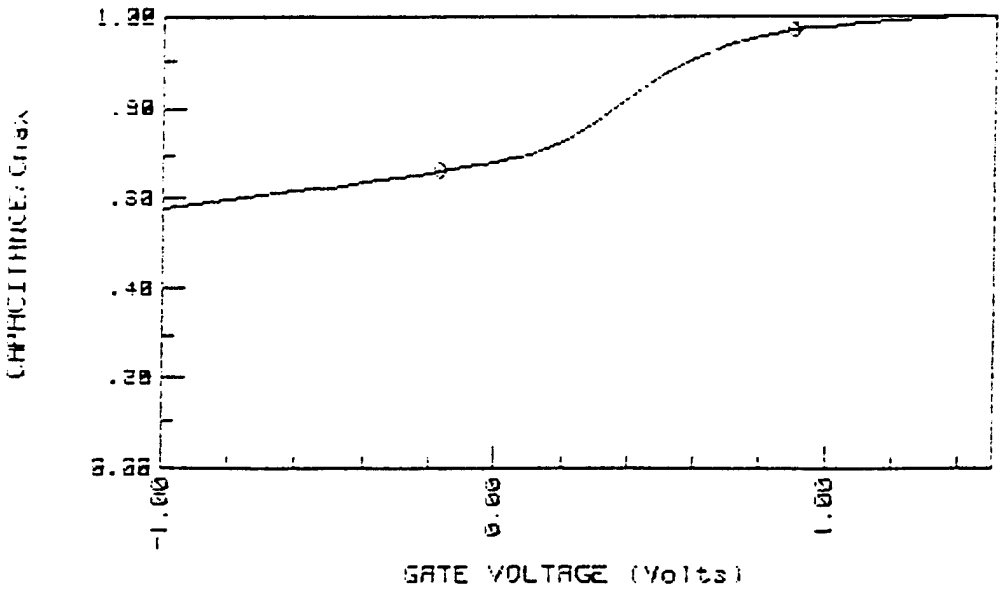

Figure 1. High frequency C-V curve for a typical Al/AlN/SiC diode. The AlN thickness is 1000 Å.

The leakage current was reduced by increasing the AlN thickness to 2500 Å. In this case, both the high frequency and the quasistatic C-V curves were measured. Figure 2 shows both of these curves on the same graph. At this thickness, the samples had low leakage currents (Fig. 3) but still did not undergo inversion.

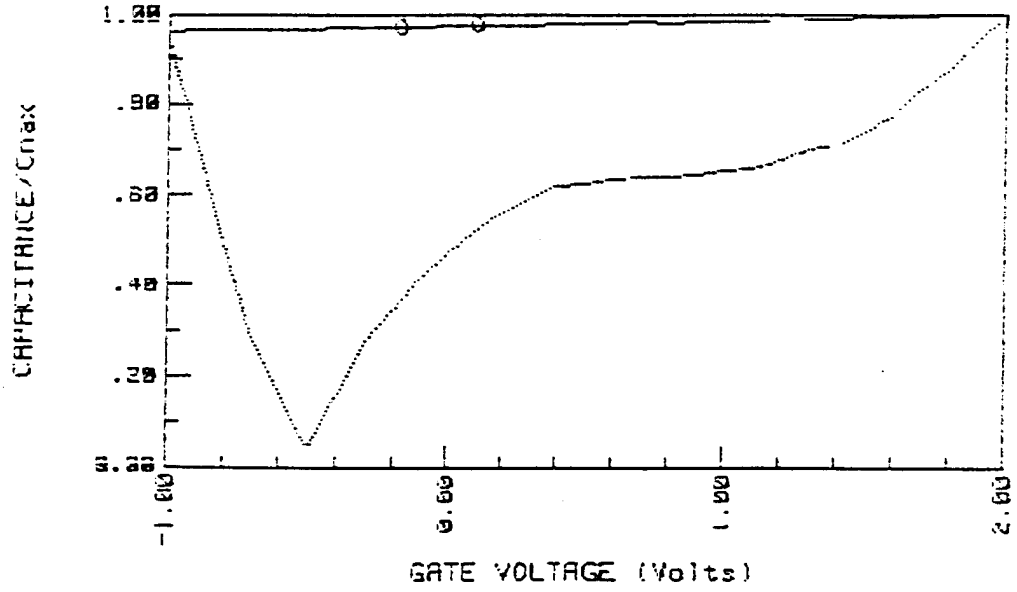

Figure 2. High frequency (solid line) and quasistatic (dotted line) C-V curves for an Al/AlN/SiC diode. The AlN thickness is 2500 Å.

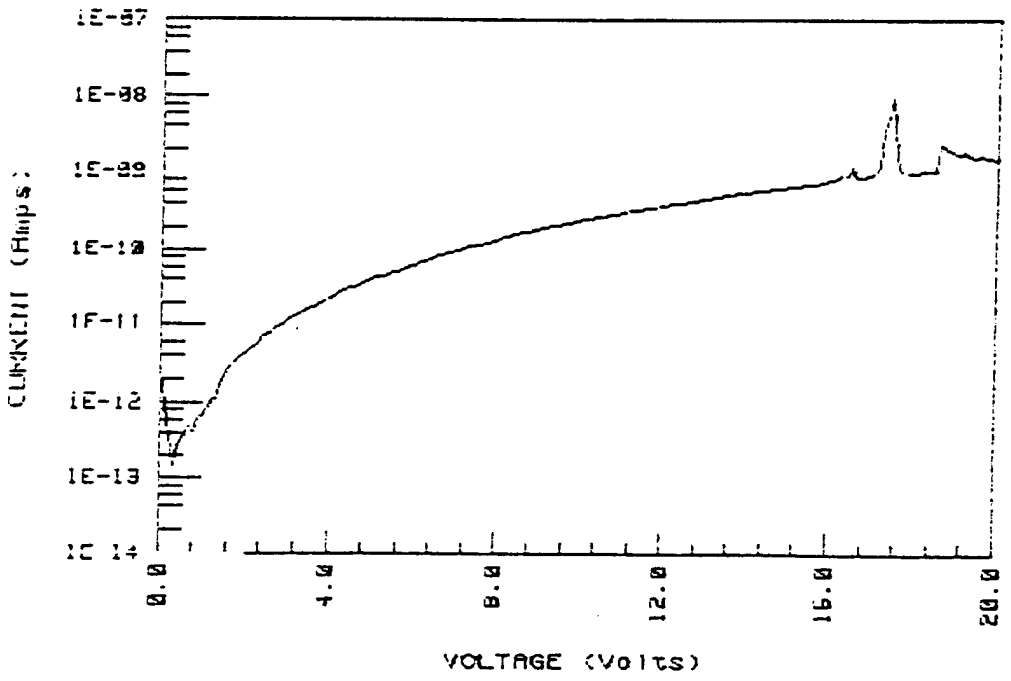

Figure 3. I-V curve for an Al/AlN/SiC diode. The AlN thickness is 2500 Å.

An interesting result of this work was that the capacitance showed a large dependency on applied frequency. When different frequencies were applied, the measured insulator capacitance was different each frequency.

D. Discussion

Figures 1 and 2 show the accumulation and depletion of Al/AlN/SiC diodes. Attempts to invert these samples at room temperature were unsuccessful. This is due to several factors. The extremely low intrinsic carrier concentration in SiC ($\approx 10^{-6}$ cm^{-3}) and the low carrier generation significantly reduce the number of minority carriers available in the SiC surface region. Despite the inability to measure the interface state density due to the leakage in the insulator, the presumed high concentration of these states as well as traps and defects in the SiC (independent of the AlN insulator) may also prevent inversion. Thicker AlN layers show better leakage characteristics and may be necessary to achieve excellent insulating properties. The dependence of the capacitance on frequency implies a relationship between dielectric constant and frequency as well since the capacitance and the dielectric constant are related by insulator thickness only.

E. Conclusions

Thin AlN insulating layers on SiC have been used in MIS structures. The resulting diodes can be accumulated and depleted but cannot be inverted by high frequency C-V characterization. Layers thinner than 1000 Å are too leaky to perform quasistatic measurements to determine the density of interface states. A large dependency of AlN dielectric constant on frequency was also observed.

F. Future Research Plans and Goals

The first priority is to reduce the leakage current and make accurate measurements of the interface state density. This will be accomplished by growing thicker layers (≈3000 Å) of AlN on the same substrates and repeating the measurements. The second priority is to achieve inversion of the semiconductor. Effects of temperature and illumination will be determined.

G. References

1. R. B. Campbell and H.-C. Chang, in *Semiconductors and Semimetals, Vol. 7B*, edited by R. K. Willardson and A. C. Beer (Academic Press, New York, 1971), p. 625.
2. W. von Muench and I. Pfaffeneder, J. Appl. Phys. **48**, 4831 (1977).
3. W. von Muench and E. Pettenpaul, J. Appl. Phys. **48**, 4823 (1977).
4. G. A. Slack, J. Appl. Phys. **35**, 3460 (1964).
5. R. F. Davis, J. W. Palmour and J. A. Edmond, Mater. Res. Soc. Symp. Proc. **162**, 463 (1990).
6. R. F. Davis, in *The Physics and Chemistry of Carbides; Nitrides and Borides*, edited by R. Freer (Kluwar Academic Publishers, The Netherlands, 1990), p. 589.
7. R. F. Davis, G. Kelner, M. Shur, J. W. Palmour and J. A. Edmond, Proc. IEEE **79**, 677 (1991).
8. R. F. Davis, J. W. Palmour and J. A. Edmond, Diam. Rel. Mater. **1**, 109 (1992).
9. R. F. Davis, Phys. B **185**, 1 (1993).
10. P. A. Ivanov and V. E. Chelnokov, Semicond. Sci. Technol. **7**, 863 (1992).
11. J. A. Powell, P. G. Neudeck, L. G. Matus and J. B. Petit, Mater. Res. Soc. Symp. Proc. **242**, 495 (1992).
12. K. Shibahara, S. Nishino and H. Matsunami, Jpn. J. Appl. Phys. **23**, L862 (1984).
13. R. E. Avila, J. J. Kopanski and C. D. Fung, Appl. Phys. Lett. **49**, 334 (1986).
14. S. M. Tang, W. B. Berry, R. Kwor, M. V. Zeller and L. G. Matus, J. Electrochem. Soc. **137**, 221 (1990).
15. M. Shinohara, M. Yamanaka, S. Misawa, H. Okumura and S. Yoshida, Jpn. J. Appl. Phys. **30**, 240 (1991).
16. C. Raynaud, J.-L. Autran, J.-B. Briot, B. Balland, N. Bécourt and C. Jaussaud, J. Electrochem. Soc. **142**, 282 (1995).
17. R. W. Kee, K. M. Geib, C. W. Wilmsen and D. K. Ferry, J. Vac. Sci. Technol. **15**, 1520 (1978).
18. R. Berjoan, J. Rodriguez and F. Sibieude, Surf. Sci. **271**, 237 (1992).
19. C. Raynaud, J.-L. Autran, B. Balland, G. Guillot, C. Jaussaud and T. Billon, J. Appl. Phys. **76**, 993 (1994).
20. C. Raynaud, J.-L. Autran, F. Seigneur, C. Jaussaud, T. Billon, G. Guillot and B. Balland, J. Phys. III **4**, 937 (1994).
21. A. Rys, N. Singh and M. Cameron, J. Electrochem. Soc. **142**, 1318 (1995).
22. J. N. Shenoy, G. L. Chindalore, M. R. Melloch, J. A. Cooper, Jr., J. W. Palmour and K. G. Irvine, J. Electron. Mater. **24**, 303 (1995).
23. G. E. Morgan, C. C. Tin, J. R. Williams and R. Ramesham, in *Silicon Carbide and Related Materials*, edited by M. G. Spencer, R. P. Devaty, J. A. Edmond, M. A. Khan, R. Kaplan, and M. Rahman (Institute of Physics, Bristol, 1994), p. 645.
24. W. M. Yim, E. J. Stofko, P. J. Zanzucchi, J. I. Pankove, M. Ettenberg and S. L. Gilbert, J. Appl. Phys. **44**, 292 (1973).
25. M. G. Norton, P. G. Kotula and C. B. Carter, J. Appl. Phys. **70**, 2871 (1991).
26. G. A. Slack, J. Phys. Chem. Solids **34**, 321 (1973).
27. J. K. Liu, K. M. Lakin and K. L. Wang, J. Appl. Phys. **46**, 3703 (1975).
28. M. Morita, N. Uesugi, S. Isogai, K. Tsubouchi and N. Mikoshiba, Jpn. J. Appl. Phys. **20**, 17 (1981).
29. G. D. O'Clock, Jr. and M. T. Duffy, Appl. Phys. Lett. **23**, 55 (1973).

VI. Distribution List

	Number of Copies
Dr. Yoon Soo Park Office of Naval Research Applied Research Division, Code 1261 800 N. Quincy Street Arlington, VA 22217-5660	3
Administrative Contracting Officer Office of Naval Research Regional Office Atlanta 101 Marietta Tower, Suite 2805 101 Marietta Street Atlanta, GA 30332-0490	1
Director Naval Research Laboratory ATTN: Code 2627 Washington, DC 20375	1
Defense Technical Information Center Bldg. 5, Cameron Station Alexandria, VA 22304-6145	2